Wear 528–529 (2023) 204975

Contents lists available at ScienceDirect

Wear

journal homepage: www.elsevier.com/locate/wear

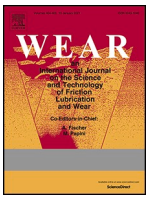

From atomic attrition to mild wear at multi-asperity interfaces: The wear of *hard* Si_3N_4 repeatedly contacted against *soft* Si

Cyrian Leriche [a,b,*], Chen Xiao [a], Steve Franklin [a,c], Bart Weber [a,b]

[a] Advanced Research Center for Nanolithography (ARCNL), Science Park 110, 1098 XG, Amsterdam, the Netherlands
[b] Van der Waals-Zeeman Institute, Institute of Physics, University of Amsterdam, Science Park 904, 1098 XH, Amsterdam, the Netherlands
[c] Department of Materials Science and Engineering, The University of Sheffield, Sheffield, UK

ARTICLE INFO

Keywords:
Topographical diffference method
Multi-asperity wear
Atomic attrition
Ductile removal
Interdependent neighboring asperities' wear

ABSTRACT

Wear causes surfaces to be irreversibly damaged, thereby incurring significant economic cost, for instance in the semiconductor industry. Much progress has been made in describing wear at single asperity interfaces between silicon based materials (Si, SiO_x, Si_3N_4), translating the fundamental understanding of wear into wear predictions and control over wear. Yet, predicting and controlling wear at industrially relevant multi-asperity interfaces remains a challenge, especially when considering the wear of the harder material subjected to repeated, nanometric scale displacement. We studied pre-sliding Si_3N_4-on-Si wear using the atomic force microscopy topography difference method and showed that the harder Si_3N_4 wears through either atomic attrition or ductile removal enhanced by subsurface damage, depending on the magnitude of the local Si_3N_4-on-Si contact pressure. Our methods and results bridge fundamental insight into wear based on nanoscale studies to industrial applications.

1. Introduction

Industrialized nations have been estimated to spend more than 4% of their gross national product on replacing worn surfaces [1–3]. The wide use of silicon-based materials in cutting tools, MEMS/NEMS and other industrial applications [4–7] is motivated by the high wear resistance of these materials. Nevertheless, silicon-based components wear and need to be replaced, even if they are harder than the material they contact [8,9]. Precision positioners are routinely used to clamp samples, but the process of clamping can cause nanometer-scale slip due to small misalignments between the surfaces. These interactions typically involve *hard* and wear-resistant positioner surfaces coming into contact with *softer* sample backsides. Despite their importance in the semiconductor industry, the mechanisms that drive positioner wear under such conditions are still unclear. Friction and wear can significantly impact precision positioning, which is crucial given the ongoing shrinkage of transistors as dictated by Moore's Law. Generally, wear of multi-asperity interfaces remains difficult to predict from first principles and this lack of understanding hampers our ability to improve wear performance. The scientific challenge is to translate the growing fundamental knowledge of nanoscale wear processes [10,11] into predictive understanding of multi-contact wear [12], which currently can only be described by empirical models.

For nanoscale single asperity silicon contacts, atomic attrition [13–15] driven by mechanochemistry [16–20] has been shown to dominate wear: stress at the interface assists the thermally activated wear process which takes place through the formation and breakage of covalent bonds. However, for multi-contact interfaces other meso-to-macro scale wear mechanisms may also occur. Depending on the precise contact conditions fatigue [21], fracture [22], (sub)-surface damage [23,24], abrasive wear [21,25] and impact wear [26–28] can become dominant wear mechanisms. The role of water at the interface can depend drastically on the contact size [21,29–32] as water sets the chemical landscape, influences adhesion and may act as a lubricant [33,34]. For macroscale experiments the Archard law [35] of wear often holds implying that the wear volume scales with the sliding distance, the applied load and the hardness of the softer material. A deeper understanding of multi-contact wear is facilitated by nanoscale wear measurements which have been achieved through the topography difference method [36–38], in which topographs recorded using Atomic Force Microscopy [36,38] (AFM) or White Light Interferometry [39] (WLI) before and after the wear experiment are subtracted to visualize wear. However, due to the use of small AFM scans or large WLI images, either the ability to capture multiple contacts or the measurement resolution

* Corresponding author. Advanced Research Center for Nanolithography (ARCNL), Science Park 110, 1098 XG, Amsterdam, the Netherlands.
E-mail address: c.leriche@arcnl.nl (C. Leriche).

https://doi.org/10.1016/j.wear.2023.204975
Received 5 January 2023; Received in revised form 1 May 2023; Accepted 21 May 2023
Available online 22 May 2023

are limited.

To model the wear behavior of precision positioning devices, we applied the topography difference method using high resolution AFM measurements [40] to the non-repeated sliding of silicon nitride (Si_3N_4) spheres of varying surface roughness against polished silicon wafers. The motivation for varying surface roughness stems from the observation that local contact pressure, which is controlled by surface roughness [41,42], can activate wear on the atomic scale [14,18,19,29,30,43–45]. The total Si_3N_4 wear volume accumulated over the full set of sliding cycles was quantified and the Si_3N_4 on Si contact pressure was calculated using an elasto-plastic boundary element model, applied to the measured topographs. The findings of our study suggest that the wear behavior of Si_3N_4 is influenced by the surface topography, with atomic scale attrition dominating for smooth interfaces and ductile removal aided by subsurface damage prevailing for rougher interfaces. Furthermore, a closer examination of individual Si_3N_4 asperities reveals that neighboring asperities exhibit mutual influence on their wear when their distance is smaller than their size, implying that they cannot be regarded as wearing independently.

2. Experimental methods

2.1. Materials

3 mm diameter Si_3N_4 spheres polished to an ISO grade 5 (root mean square height (h_{RMS}) 15–20 nm, measured by AFM on a 90 × 90 μm^2 scan) and commercially available (BC precision), were used in this work. The counter surface was a polished p-type single crystal (100) Si wafer (University Wafer) with a native oxide layer and a root mean square roughness of 1 nm (measured on a 5 × 5 μm^2 AFM scan). As mentioned in the introduction, the choice of these materials has been made based on their industrial relevance. Before each wear experiment, the spheres were cleaned using acetone and isopropanol (Sigma Aldrich) in an ultrasonic bath for 20 min in each solvent, followed by a deionized water rinse. The same cleaning procedure was used after the wear test to remove potential wear debris from the surface.

2.2. Methods

2.2.1. Samples: Si_3N_4 spheres with varying roughness

3 mm diameter Si_3N_4 spheres were roughened to various degrees. Two methods were employed to achieve increased surface roughness; (i) The pristine sphere was placed in a plastic cylindrical tube (15 cm high, 3 cm diameter) together with a double-sided piece of sand paper (3 × 3 cm^2, corundum particle size from 162 μm to 8 μm, tailored to the shape and size of the tube so that it could not move) and the tube was subsequently inserted into a vortex shaker for 5–30 h of shaking at a frequency of 2000 rotations per minute. Collisions of the sphere onto the sand paper induced by the vortex shaker damage the sphere surface, increasing the h_{RMS} surface roughness up to 250 nm (measured by AFM on a 90 × 90 μm^2 area). (ii) Pristine spheres were subjected to a sand blasting procedure (0.8 μm particle size, 1, 2 and 3 bar of pressure for 5 s). The sand particles colliding with the sphere surface create sharp roughness peaks, resulting in an h_{RMS} roughness of up to 500 nm (measured by AFM on a 90 × 90 μm^2 area). The pristine material properties of the Si_4N_3 – Si pair, as measured by nanoindentation (Femtotools FT-I04) are reported in Table 1.

Table 1
Material properties of Si_3N_4 and Si measured by nanoindentation (FT-I04 from Femtotools).

Materials	Young's modulus (GPa)	Poisson's ratio	Hardness (GPa)
Si_3N_4 sphere	270 ± 12	0.17	22.3 ± 1.5
Si wafer	130 ± 3	0.2	10.9 ± 0.3

2.2.2. Wear experiment

The wear experiments were performed using a Universal Mechanical Tester (UMT, Bruker TriboLab). Si_3N_4 sphere-on-Si flat wear experiments were conducted in a 'non-repeated' fashion (Fig. 1): in each sliding cycle the Si_3N_4 sphere was brought into contact with a previously untouched section of the Si substrate [46]. The wear test consisted of 2000 cycles, split into 20 series of 100 cycles (Fig. 1). At the beginning of each series the sphere was brought into contact with the wafer at a velocity of 1 μm/s until a normal force of 0.1 N was applied, after which 10 μm tangential slip was imposed. In the remaining 99 cycles of each series the same normal force was applied but the tangential displacement (and thus force) was limited such that only minimal pre-sliding [47] took place. Non-repeated wear is important for positioning applications in which wear resistant materials are repeatedly contacted by fresh samples. Varying the stroke length enables an analysis of the importance of the frictional energy dissipation in generating wear, as will be discussed later in the text. The total number of cycles was chosen such that significant wear could be detected through the topography difference method. The pre-sliding distance in the short stroke cycles is estimated to be less than 50 nm based on imaging of the wear scars on the Si substrates, which will be further discussed below. The tangential velocity with which the slider was driven in all cycles was 7 μm/s. Experiments were performed in an ambient environment: 20–22 °C, 40–60% relative humidity (RH). Force and position data were acquired at a rate of 5 Hz.

2.2.3. Imaging the Si_3N_4 sphere topographies

An AFM (Dimension ICON, Bruker) was used in tapping mode [48] to collect 90 × 90 μm^2 measurements of the sphere apex topography (Fig. 1). Topography measurements were performed before and after the wear test [40]. The measured topographs were processed using Gwyddion [49] software. Measurement artifacts (grains, line scars) were corrected and a polynomial background was removed to flatten the topography. The roughness of each sample was extracted from these measurements and defined as the standard deviation from the mean height of the surface (h_{RMS}).

2.2.4. Aligning Si_3N_4 sphere topography measurements, quantifying wear and uncertainty in wear measurements

Matlab scripts were developed to align the topography measurements [40] (Fig. 2a). The difference map was defined as the *after* topography minus the *before* topography (Fig. 2b). The alignment is based on negative heights only as they represent the unworn part of the surface.

For each sample, a control measurement was performed in which the sample is repositioned in the AFM but not worn; the standard deviation of the pixel heights in the corresponding difference map ($h_{RMS\text{-}diff\text{-}control}$) quantifies the quality of the alignment and the repeatability of the topography measurement. To disregard most of the false wear visible in the difference image we define a threshold $T_{wear} = \pm 2 \times h_{RMS\text{-}diff\text{-}control}$.

As described in Ref. [40], pixels in the difference images only count towards the measured wear if the (absolute value of the) pixel height is larger than the threshold, T_{wear}. The wear error is defined as the wear measured in the control measurement. Wear that results from local height changes larger than T_{wear} (Fig. 2b), leads to an overall wear volume -over the full contact area- ($V_{wear\text{-}full}$) significantly larger than the wear error and can be reliably detected.

The wear on all sphere surfaces ($V_{wear\text{-}full}$) was quantified using this method, as shown in Fig. 2 d. Additionally, the method was used to analyze the indentation marks left on the flat silicon wafer after being contacted by the roughest Si_3N_4 sphere ($V_{asp\text{-}wear}$), as depicted in Fig. 3. This analysis indirectly provides information on the wear of the rough Si_3N_4 asperities during the wear experiment, as the indentation marks on the wafer can be interpreted as *footprints* of the Si_3N_4 asperities.

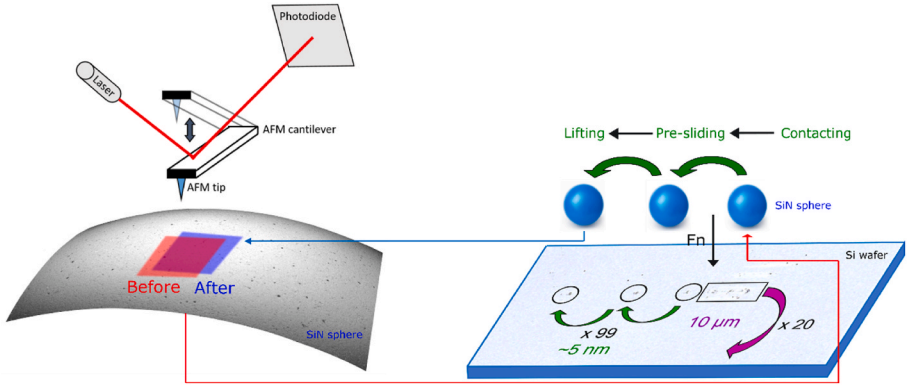

Fig. 1. Schematic of the topography and wear measurements (image based on Ref. [40]). The Si_3N_4 sphere apex is imaged (90 × 90 µm^2, left hand side), using an AFM in tapping mode before and after the wear experiment. The wear experiment consists of 2000 'non-repeated' strokes which can be subdivided into 20 series of 100 strokes. The first stroke in each series covers a sliding distance of 10 µm (rectangle, right hand side). The 99 subsequent strokes in each series (circles, right hand side) take place in the pre-sliding regime [51–53]; based on Fig. 3, the short stroke slip distance is less than 50 nm. The normal force in all cycles is 100 mN.

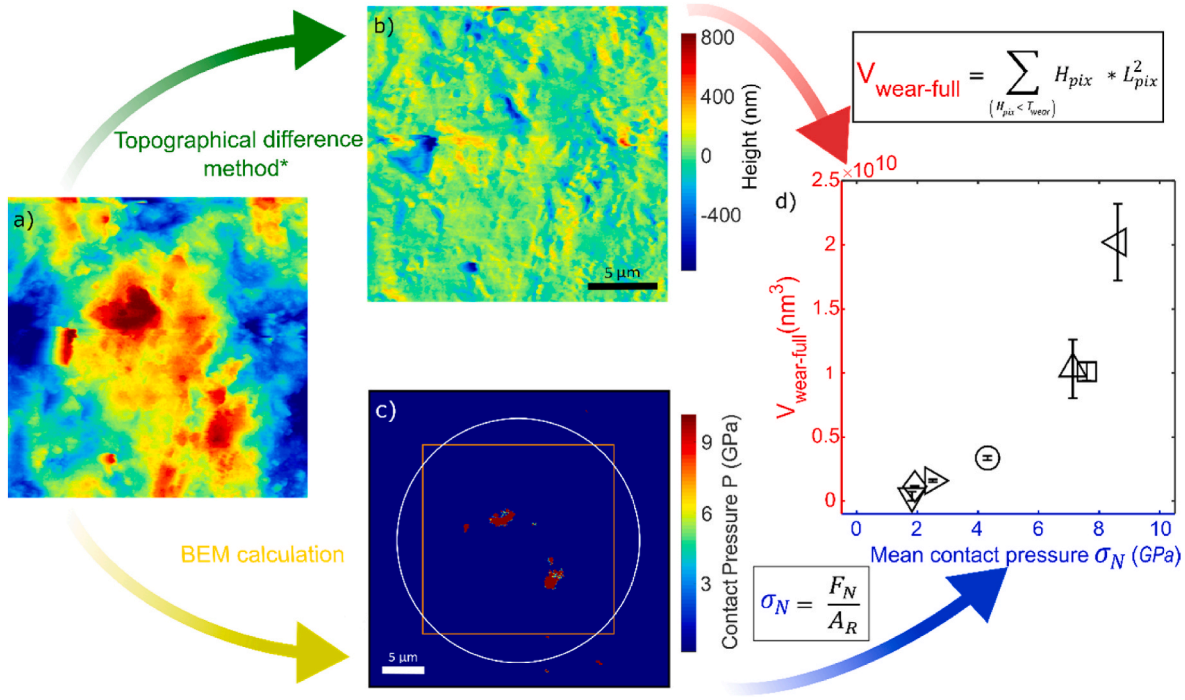

Fig. 2. Wear and mean contact pressure quantification at multi asperity interfaces. a) AFM image of the sphere topography before the wear test. b) Difference image obtained by subtracting the *before* topography from the *after* topography (negative heights represent the material that has been removed from the surface (blue)). As the areas with negative height in (b) represent a larger volume than those with positive height, Si_3N_4 was worn off the sphere surface. c) Boundary Element Method (BEM) contact calculation based on the *before* topography from a). The white circle in c) represents the Hertzian contact area and the orange square represents the area to which the topography difference method was applied. d) Si_4N_3 wear volume, $V_{wear\text{-}full}$, measured over the full contact area over all cycles vs the average contact pressure, $\sigma_N = F_N/A_R$: the procedure described in a), b) and c) is repeated for 7 Si_3N_4 spheres with varying roughness. (For interpretation of the references to colour in this figure legend, the reader is referred to the Web version of this article.)

2.2.5. Contact calculations

Contact calculations using the Tribology Simulator (www.tribology.org) were employed to estimate the average contact pressure exerted at the interface between the Si_3N_4 sphere asperities and the Si flat (Fig. 2c). The half-space contact calculations were based on the boundary element method (BEM) [50], whereby the elasto-plastic deformation of asperities at the interface was solved. In the calculation, strain hardening is assumed to be negligible, and the contact pressure is limited by the hardness of the softest material. The contact calculations were carried out at a nominal pressure of 163 MPa, in accordance with the nominal pressure in the experiments as calculated using Hertz theory (white circle in Fig. 2c). Cropped, 40 × 40 µm^2 (440 × 440 pixels) topographs were used as input for the calculations. It is important to note that there is a small misalignment between the orientation of the Si_3N_4 sphere in the contact calculation compared to the orientation of the Si_3N_4 sphere in the wear experiment, causing the collection of contacting asperities in the calculation to be slightly different from that in the wear experiment. The normal force divided by the area of real contact, A_R, which is given by the pixels with non-zero contact pressure in Fig. 2c, gives the mean contact pressure at the interface which is reported in Table 2.

3. Results

Table 2 displays the roughness, calculated mean contact pressure and Si_4N_3 wear volume, $V_{wear\text{-}full}$, for all Si_3N_4 spheres with which wear experiments were conducted. Spheres with more surface roughness generate a larger contact pressure because the load exerted at these interfaces is carried within a smaller contact area. Surprisingly, the wear volumes reported in Table 2 vary by a factor 36 when comparing the smoothest (least worn) and the roughest (most worn) Si_3N_4 spheres,

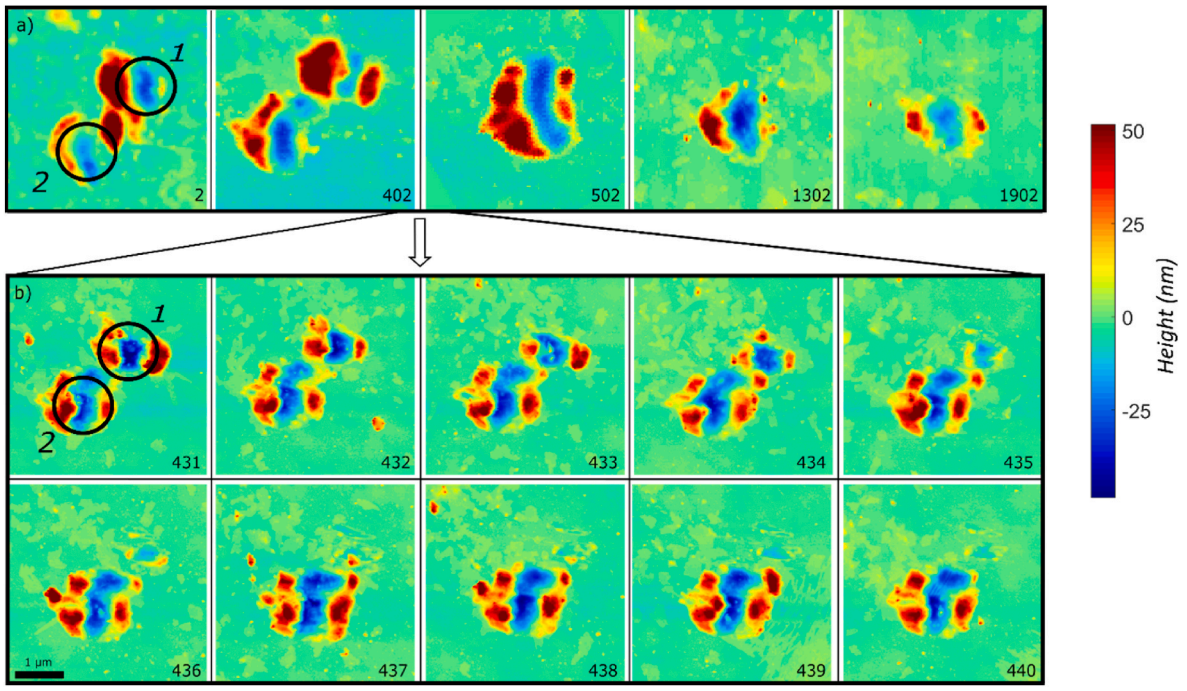

Fig. 3. Indentations left on the Si wafer after the wear experiment. The local wear of the Si_3N_4 sphere (h_{RMS} = 431 nm) can be tracked over the full wear experiment through the indentations (Si_3N_4 sphere 'footprints') left on the Si wafer. a) Evolution of the wear scar from cycle 2 to 1902. b) Sequence of indentations made during cycle 431 to 440, indirectly displaying gradual wear of the Si_3N_4 asperities. The pre-sliding direction was toward the right. The lack of directionality/scratches in the wear scars indicates that the sliding distance remained below 50 nm. However, we do expect a finite amount of slip to take place because both theoretical and experimental evidence suggest that partial slip at the nanometer scale takes place at tangential forces well below the dynamic friction force [47,54].

Table 2
Roughness, contact pressure and Si_4N_3 wear volume, measured over the full contact areas over all cycles. Root mean square roughness, h_{RMS}, was calculated using the 90 µm × 90 µm AFM topography measurements. The mean contact pressure was obtained from the contact calculations. The wear volumes induced by the wear experiment were analyzed using the topography difference method [40].

Sample roughness (h_{RMS}) in nm	Mean contact pressure in GPa	$V_{wear\text{-}full}$ in mm^3
9.9 (v)	1.7 GPa	$6.7\ 10^{-10} \pm 2.6\ 10^{-10}$
16 (d)	1.8 GPa	$9.9\ 10^{-10} \pm 4.9\ 10^{-11}$
62.9 (>)	2.2 GPa	$1.4\ 10^{-9} \pm 8.1\ 10^{-11}$
176.3 (o)	4.2 GPa	$3.8\ 10^{-9} \pm 1.4\ 10^{-10}$
135.8 (^)	7.0 GPa	$1.3\ 10^{-8} \pm 1.8\ 10^{-9}$
131.8 (s)	7.4 GPa	$1.1\ 10^{-8} \pm 5.5\ 10^{-10}$
431 (<)	8.5 GPa	$2.4\ 10^{-8} \pm 2.3\ 10^{-9}$

even though all spheres were subjected to exactly the same wear experiment. The mean contact pressure calculated for each type of sphere, however, differs by a factor 5. The exponential increase in measured Si_4N_3 wear volume ($V_{wear\text{-}full}$) with the mean contact pressure is plotted in Fig. 2d. To better understand the underlying wear mechanism(s), we also analyze the wear scars left on the Si substrate after the wear experiment.

As the h_{rms} = 431 nm Si_3N_4 sphere makes contact with the Si substrate, the sharp Si_3N_4 asperities can plastically indent the Si substrate, leaving behind 'footprints' of the Si_3N_4 asperities in each cycle of the experiment as well as pile-up of Si material around the indentations. The evolution of the indentations as a function of cycle number, and thus the shape of the Si_3N_4 asperities causing these indentations, is shown in Fig. 3.

Fig. 3a shows the indentation mark caused by two neighboring asperities on the Si_3N_4 surface. As the asperity responsible for the upper right indentation mark (*1* in Fig. 3) wears between cycle 402 and 502, its neighbor (*2* in Fig. 3) takes on more load resulting in larger indentations on the wafer. Indeed the detailed imaging confirms that the upper right asperity *1* is gradually worn between cycle 431 and 440, after which the local pressure exerted by the asperity on the Si wafer no longer leads to plastic deformation. Fig. 4 shows how asperity *2* takes over extra interfacial load as asperity *1* wears, which results in a deeper and wider indentation, in turn enhancing the wear of asperity *2*. These observations demonstrate that there are asperity scale interactions; individual asperities cannot be assumed to wear independent of their neighbors.

The wear behavior detailed in Fig. 3b suggests that the indentation volume and area gradually decrease as the experiment progresses. To further confirm this, the first and last indentation mark of each of the 20 series of 99 short strokes were imaged. Thus, the asperity scale Si_3N_4 wear volume ($V_{asp\text{-}wear}$) accumulated during 99 short strokes or 1 long stroke could be calculated by applying the topographical difference method [40] to the indentation marks. The positive heights (red pile-up material in Fig. 3) were set to 0 height to align only over the asperity shaped features. To obtain the Si_3N_4 asperity scale wear volume accumulated during 99 short strokes, the first indentation mark in a series was subtracted from the last indentation mark in that same series (green circles Fig. 5). The Si_3N_4 asperity scale wear volume accumulated during a single 10 µm stroke was calculated by subtracting the indentation recorded directly before that long stroke from the indentation recorded directly after the long stroke (magenta squares, Fig. 5).

The results reported in Figs. 3–5 lead to three important observations: (i) The Si_3N_4 wear rate drops during the experiment by a factor 3–4. This is a small reduction compared to the factor 36 difference in wear rate observed as the contact pressure is varied in Fig. 2. However, in agreement with the results reported in Fig. 2, the wear rate likely drops during the experiment because the contact pressure drops; the gradual smoothening of Si_3N_4 asperities results in a reduction in the mean contact pressure across the interface. Nonetheless, wear is distributed relatively (within a factor of 3–4) homogeneously over the cycles. (ii) The indentation area (blue 'foot-print' area of the Si_3N_4

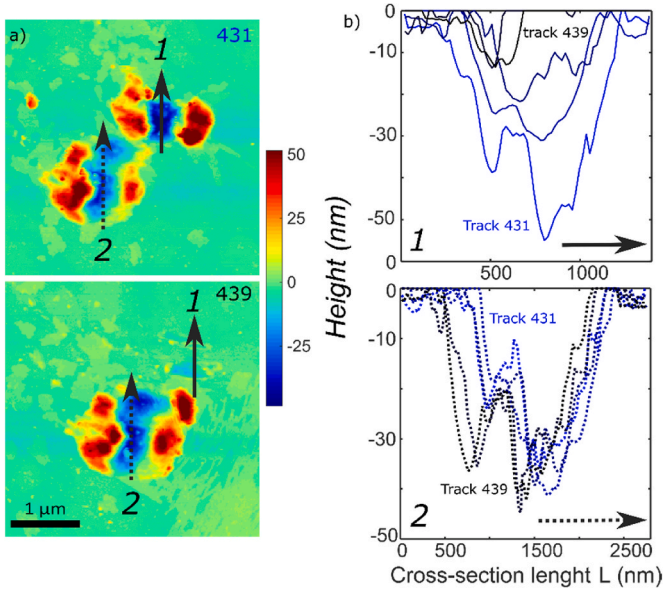

Fig. 4. Evolution of the indentation marks between track 431 and 439, shown as topographs (a) and as cross sections (b) along the profiles in (a). While indentation *1* (also displayed in Fig. 3) disappears in the course of the experiment, indentation *2* (also displayed in Fig. 3) becomes wider and deeper. As the Si_3N_4 asperity responsible for indentation *1* wears, the asperity responsible for indentation *2* takes on more load.

sphere in Fig. 3) carries a large fraction of the total load and decreases homogeneously with the number of cycles, indicating that the area within which the contact pressure is sufficiently large to result in plastic deformation of the Si substrate shrinks as the experiment progresses (Figs. 3–5); this confirms that the contact pressure decreases as the wear progresses. (iii) Surprisingly, short strokes contribute more strongly to the total wear than long strokes; the sum of the local Si_3N_4 wear volumes

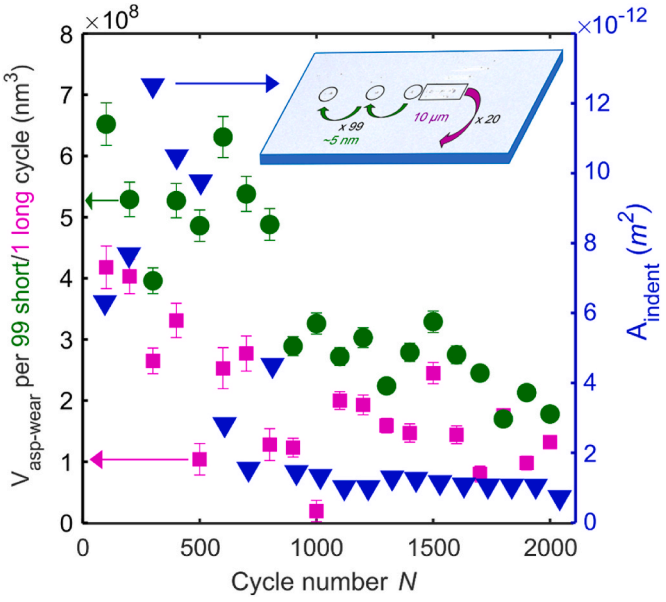

Fig. 5. Asperity scale Si_3N_4 wear volume throughout the wear experiment, measured by applying the topography difference method to subsequent indentations left on the Si wafer (see main text and Fig. 3). The asperity scale Si_3N_4 wear volume accumulated during each series of 99 short strokes (green circles, total sliding distance less than: 50 nm x 99 = 4950 nm) decreases as the experiment progresses. Similarly, asperity scale Si_3N_4 wear volume incurred per 10 µm (10.000 nm) stroke decreases as the experiment progresses (magenta squares). The blue triangles represent the indentation area (blue areas in Fig. 3 a and b). (For interpretation of the references to colour in this figure legend, the reader is referred to the Web version of this article.)

observed during short strokes in Fig. 5 accounts for about 70% of the total Si_3N_4 wear volume measured in Fig. 2 (for the h_{RMS} = 431 nm sample). This observation confirms that the wear measured directly on the Si_3N_4 sphere using the topography difference method matches the Si_3N_4 wear inferred indirectly through the Si wear scars. Furthermore, this observation indicates that the Si_3N_4 sphere is primarily worn at those locations where it plastically indents the Si wafer.

Fig. 5 shows that the wear rate of Si_3N_4 at the asperity scale decreases by a factor of three during the wear experiment, for both short and long sliding cycles. While this reduction may seem significant, it is relatively small compared to the substantial impact of surface roughness on the overall wear volume of Si_3N_4 across the entire contact area and over all sliding cycles. Fig. 2 indicates a strong dependence of wear volume on surface roughness, with a variation of up to a factor of 36. This observation highlights the need for further analysis of the mean Si_3N_4 wear per cycle.

To analyze this further, we normalize the total Si_3N_4 wear volume ($V_{wear\text{-}full}$) by the total number of short stroke cycles (1980), since most Si_3N_4 wear occurs during the short strokes. Then, we can divide this average Si_3N_4 wear volume per cycle by the area of real contact (A_R), which is the result of BEM calculation for each sample. The resulting value provides the average thickness of Si_3N_4 material removed from the sphere within the area of real contact per short stroke cycle (as shown in Fig. 6). We find that the average thickness of the layer of removed Si_3N_4 material is only 6 p.m. for the smoothest sample but increases exponentially with increasing contact pressure to 1 nm for the roughest sample. As 6 p.m. represents only a small fraction of an atomic monolayer thickness, this removal rate observed in the low contact pressure experiments is consistent with atomic attrition [14,17,43,55] in which the stochastic formation and rupture of interfacial siloxane bonds drives the wear process. However, wear mechanisms occurring at a larger scale, further discussed in the next sections, play a role of increasing importance in the high contact pressure experiments.

4. Discussion

1. Atomic attrition at contact pressures below 5 GPa

At local contact pressures below 5 GPa, the average thickness of the

Si_3N_4 layer worn off the sphere per sliding cycle ranges from 6 to 100 p.m., strongly suggesting that atomic attrition is the dominant wear mechanism. Our observations coincide with model predictions of atomic attrition through interfacial siloxane bonds [19] and match the experimental results obtained using single asperity contacts between silicon based materials [14,43]; in these models and experiments a layer thickness of approximatively 2–50 p.m. is worn off when the contact slides by a distance comparable to its size (10–50 nm). Furthermore, a mean removal layer per stroke ranging from about 10 to 100 p.m. was found for AFM colloidal probe wear experiments (500 nm stroke length on a contact of about 50–100 nm), in which the wear was attributed to atomic attrition [17,55,69].

2. Mild wear enhanced by subsurface damage at contact pressures above 5 GPa

Figs. 3–5 indicate that at contact pressures above 5 GPa, Si_3N_4 wear occurs gradually, yet involves the removal of layers of 0.1–1 nm of Si_3N_4 material, involving more than a single layer of atoms. The wear mechanism in these experiments most likely involves ductile removal [56,57] enhanced by subsurface damage of the Si_3N_4, unlike the atomic attrition process that dominates at pressures below 5 GPa and only occurs at the surface.

In all wear experiments we observe a decrease of the Si_3N_4 sphere surface roughness as the wear progresses, consistent with the behavior found in molecular dynamics simulations under similar conditions [41]. In accordance with those simulations, we observe that at high contact pressures, the smoothening of the Si_3N_4 surface leads to a decrease in the local contact pressure [58]. As the local contact pressure drops, the amount of Si_3N_4 material removed in subsequent sliding cycles also reduces. Moreover, we observe asymptotic evolution of both the wear rate and the indentation area (Fig. 5) which is typical for running-in behavior [59–61]. It should be noted that the gradual reduction in indentation area observed in Fig. 5 does not imply that the area of real contact decreases, only that the area within which the contact pressure exceeds the hardness of the Si decreases. The fact that the indentations not only change in terms of their depth but also in terms of their shape as the wear experiment progresses, demonstrates that interactions between asperities, influenced by the varying asperity level wear rate, take place. Local asperity wear influences the load distribution and thus the local wear rate (Fig. 4). Such asperity interactions [62,63] are typically not taken into account yet in theoretical descriptions of multi-contact wear [64]. Systematic manipulation of the size of and distance between asperities is a promising avenue for future experimental research into the role of asperity interactions in wear [65].

The roughening treatment to which the Si_3N_4 surfaces that exerted contact pressures larger than 5 GPa were subjected may have played a role in the wear process; the crystal and/or amorphous [24] structure of the (oxidized) Si_3N_4 surface may have been weakened by the roughening procedure. This hypothesis could be tested in future work by annealing the roughened surfaces before conducting the wear experiments [66]. Nanoindentation measurements on the Si_3N_4 spheres, performed after the wear experiments (Femtotools FT-I04 equipped with FT S-200000 MEMS force sensors) indicate that indeed the hardness of the Si_3N_4 surface decreases significantly due to the sand blasting roughening procedure while the vortex shaking procedure does not produce a measurable change in surface hardness (Supplementary Fig. 1). This interplay between surface manipulation technique and wear behavior is important to consider in future attempts at systematically investigating multi-contact wear as a function of contact geometry. Furthermore, these results highlight that surface preparation can play a key role in wear behavior.

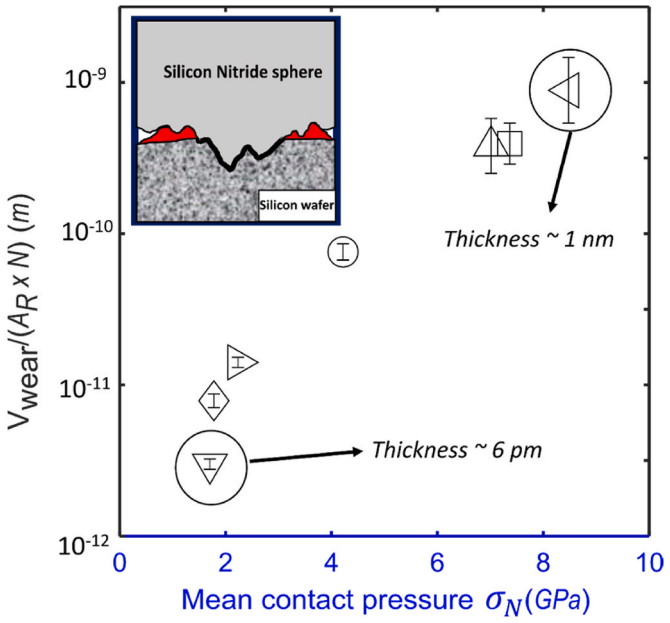

Fig. 6. Average thickness of the layer of removed Si_3N_4 material per short stroke cycle as a function of the average contact pressure within the area of real contact. The Si_3N_4 wear volumes ($V_{wear\text{-}full}$) obtained through the topographical difference method and presented in Fig. 2 are normalized by the area of real contact obtained in the BEM calculations, A_R, and by the total number of short stroke cycles in the wear experiment (1980). Inset: side view illustration of a Si_3N_4 asperity indenting the Si wafer creating Si pile up material (red) and wearing off a layer of Si_3N_4 (thick black line). (For interpretation of the references to colour in this figure legend, the reader is referred to the Web version of this article.)

3 Short stroke vs long stroke wear

Surprisingly, analysis of the energy dissipation, $E = F_f d$, with E the energy dissipated through the friction force F_f over sliding distance d, shows that at least 26 times more energy is dissipated through friction during one long stroke ($E = F_f d = 7 \bullet 10^{-2} \bullet 10^{-5} = 7 \bullet 10^{-7} J$) than during 99 short strokes ($E = 99 F_f d = 99 \bullet 5 \bullet 10^{-3} \bullet 50 \bullet 10^{-9} = 2,5 \bullet 10^{-8} J$). Yet the short strokes lead to 70% of the total wear observed (Figs. 2 and 5). In addition to the energy dissipated through slip, the lifting of the Si_3N_4 sphere from the Si wafer after each cycle also contributes to energy dissipation. A rough estimate of the energy dissipated during unloading can be obtained by multiplying the area of real contact with a typical surface energy of $\gamma = 50\, mJ/m^2$, resulting in an energy dissipation of $E = \gamma \bullet A_r = 5 \bullet 10^{-13} J$: this energy is orders of magnitude lower than the energy dissipated through friction. Another source of energy dissipation is during the contact formation or impact [28] of the Si_3N_4 sphere onto the Si wafer. While previous studies have focused on how impact energy is dissipated through plastic deformation or fracture of the softer material [26–28,67], the impact energy can potentially also contribute to the wear of the harder Si_3N_4 surface by weakening it. However, it is difficult to obtain quantitative estimates of the impact energy as it depends on the masses and instrument stiffnesses involved. Therefore, future experiments with varying impact speed may provide more insight into the precise wear mechanisms at play, as the energy dissipation caused by pull-off and slip seems to be insufficient to explain the difference in wear rate observed between short and long strokes.

5. Summary and conclusion

We investigated the wear of relatively *hard* Si_3N_4 repeatedly brought into contact with previously untouched and relatively *soft* Si. Despite the contrast in hardness we found significant wear of the Si_3N_4. A large AFM scan topographical difference method was applied to quantify the Si_3N_4

wear, using a 6-degrees of freedom alignment algorithm [40]. The topographical difference method was also applied to the wear tracks on the Si wafer surface enabling visualization of the wear induced evolution of individual Si_3N_4 asperities throughout the wear experiment.

The local Si_3N_4-on-Si contact pressure was shown to play a crucial role in the wear process, by coupling the wear observations to BEM contact calculations. At contact pressures below 5 GPa, our results strongly suggest that the dominant wear mechanism is atomic attrition, potentially driven by interfacial siloxane bonds [55]. At contact pressures above 5 GPa the wear mechanism involves removal of multiple atomic layers in each contact cycle. This transition in wear behavior as a function of contact pressure is reminiscent of the adhesion induced transition in wear behavior observed in recent calculations [68], where both compressive and shear stresses played a crucial role in the wear behavior. Furthermore, our results demonstrate that the wear of individual neighboring asperities is not independent; asperity wear can influence the load distribution which in turn affects wear.

Surprisingly, the observed Si_3N_4 wear in the pre-sliding wear experiments did not scale with the energy dissipated through friction, suggesting that contact formation (impact wear) and/or pull-off (adhesive wear) played an important role in the wear process. Based on our findings the optimal Si_3N_4 topography, for minimizing wear, would be the smoothest possible. However, if the surface roughness were to be reduced to values below $h_{RMS} = 5$ nm capillary adhesion is expected to increase, leading to an increase in the effective normal force [42] which may further enhance wear. Our work contributes to a first principles description of multi-contact wear and can inspire understanding-based solutions to wear challenges in the semiconductor industry.

Declaration of competing interest

The authors declare the following financial interests/personal relationships which may be considered as potential competing interests: Bart Weber reports financial support was provided by Dutch Research Council Domain Science.

Data availability

Data will be made available on request.

Acknowledgement

Foremost, we thank Jean-François Molinari (école Polytechnique de Lausanne), Tevis Jacobs (University of Pittsburg) and Seong Kim (Pennsylvania State University) for their help to interpret and understand our results that significantly helped to improve the quality of this work. We thank Felix Cassin for his insights and ideas. We thank Feng-Chun Hsia for making two of the used samples for this study.

This work has been carried out at the Advanced Research Center for Nanolithography (ARCNL), a public-private partnership of the University of Amsterdam (UvA), the Vrije Universiteit Amsterdam (VU), the Netherlands Organisation for Scientific Research(NWO) and the semiconductor equipment manufacturer ASML. B. W. acknowledges funding from the NWO VENI grant No. VI.Veni.192.177.

Appendix A. Supplementary data

Supplementary data to this article can be found online at https://doi.org/10.1016/j.wear.2023.204975.

References

[1] Early, E. H., Jost, T., Physics, S. & Laws, F. Tribology.
[2] K. Holmberg, A. Erdemir, Influence of tribology on global energy consumption, costs and emissions, Friction 5 (2017) 263–284.
[3] K. Holmberg, A. Erdemir, Global impact of friction on energy consumption, economy and environment, FME Trans. 43 (2015) 181–185.
[4] X.S. Li, I.M. Low, Ceramic cutting tools - an introduction, Mech. Corros. Prop. Ser. A, Key Eng. Mater. 96 (1994) 1–18.
[5] A. Moulson, Herbert, J. *Electroceramics; Material, Properties, Applications*, Wiley, 2003.
[6] J. Chevalier, L. Gremillard, Ceramics for medical applications: a picture for the next 20 years, J. Eur. Ceram. Soc. 29 (2009) 1245–1255.
[7] R. Ji, et al., Optimizing machining parameters of silicon carbide ceramics with ED milling and mechanical grinding combined process, Int. J. Adv. Manuf. Technol. 51 (2010) 195–204.
[8] J. Chu, Why Shaving Dulls Even the Sharpest of Razors, MIT News Office., 2020.
[9] G. Roscioli, S.M. Taheri-mousavi, C.C. Tasan, How hair deforms steel 694 (2020) 689–694.
[10] J. Choudhry, R. Larsson, A. Almqvist, A Stress-state-dependent Thermo-Mechanical Wear Model for Micro-scale Contacts, 2022.
[11] R. Aghababaei, D.H. Warner, J.F. Molinari, Critical length scale controls adhesive wear mechanisms, Nat. Commun. 7 (2016) 1–8.
[12] S. Pham-Ba, J.F. Molinari, Adhesive wear regimes on rough surfaces and interaction of micro-contacts, Tribol. Lett. 69 (2021) 1–16.
[13] H. Bhaskaran, et al., Ultralow nanoscale wear through atom-by-atom attrition in silicon-containing diamond-like carbon, Nat. Nanotechnol. 5 (2010) 181–185.
[14] T.D.B. Jacobs, R.W. Carpick, Nanoscale wear as a stress-assisted chemical reaction, Nat. Nanotechnol. 8 (2013) 108–112.
[15] J.H. Liang, et al., Stress-dependent adhesion and sliding-induced nanoscale wear of diamond-like carbon studied using in situ TEM nanoindentation, Carbon N. Y. 193 (2022) 230–241.
[16] B. Gotsmann, M.A. Lantz, Atomistic wear in a single asperity sliding contact, Phys. Rev. Lett. 101 (2008) 1–4.
[17] C. Xiao, et al., Effect of crystal plane orientation on tribochemical removal of monocrystalline silicon, Sci. Rep. 7 (2017) 1–7.
[18] H. Spikes, Stress-augmented thermal activation: tribology feels the force, Friction 6 (2018) 1–31.
[19] Y. Shao, et al., Multibond model of single-asperity tribochemical wear at the nanoscale, ACS Appl. Mater. Interfaces 9 (2017) 35333–35340.
[20] W. Maw, F. Stevens, S.C. Langford, J.T. Dickinson, Single asperity tribochemical wear of silicon nitride studied by atomic force microscopy, J. Appl. Phys. 92 (2002) 5103–5109.
[21] M.C. Mate, R.W. Carpick, Tribology on the Small Scale - A Modern Textbook on Friction, Lubrication, and Wear, vol. 59, 2019.
[22] T.E.-4529. Fischer, Wear 105 (1985) 29–45.
[23] S. Jacobson, S. Hogmark, Surface modifications in tribological contacts, Wear 266 (2009) 370–378.
[24] H. Liu, H. Kaya, Y.T. Lin, A. Ogrinc, S.H. Kim, Vibrational spectroscopy analysis of silica and silicate glass networks, J. Am. Ceram. Soc. 105 (2022) 2355–2384.
[25] S. Jahanmir, Water lubrication of silicon nitride in sliding, Tribol. Lett. 40 (2004) 50–62.
[26] R. Lewis, A modelling technique for predicting compound impact wear, Wear 262 (2007) 1516–1521.
[27] S. Shi, et al., A comparative study on impact wear of diamond-like carbon films on H62 and GCr15 steel, J. Mater. Eng. Perform. 31 (2022) 6722–6735.
[28] P.J. Blau, Friction, lubrication and wear technology, Technology 2 (2001) 3470.
[29] M.K. Beyer, Clausen-Schaumann, H. Mechanochemistry, The mechanical activation of covalent bonds, Chem. Rev. 105 (2005) 2921–2948.
[30] J. Ribas-Arino, D. Marx, Covalent mechanochemistry: theoretical concepts and computational tools with applications to molecular nanomechanics, Chem. Rev. 112 (2012) 5412–5487.
[31] Y. Qi, et al., Investigation of silicon wear against non-porous and micro-porous SiO2 spheres in water and in humid air, RSC Adv. 6 (2016) 89627–89634.
[32] X. Dong, S. Jahanmir, Wear Transition Diagram of Silicon Nitride, vol. 5, 1993, pp. 169–180.
[33] W. Qin, W. Yue, C. Wang, Controllable wear behaviors of silicon nitride sliding against sintered polycrystalline diamond via alterning humidity, Int. J. Lab. Hematol. 38 (2018) 42–49.
[34] J. Xu, K. Kato, Formation of tribochemical layer of ceramics sliding in water and its role for low friction, Wear 245 (2000) 61–75.
[35] J. Archard, Elastic deformation and the laws of friction, Ray Soc. (1957) 190–205.
[36] R. Gahlin, A Novel Method to Map and Quantify Wear on a Micro-scale, 1998, pp. 93–102.
[37] H. Bosse, H. Kunzmann, G. Dai, F. Pohlenz, CIRP Annals - Manufacturing Technology Quantitative analysis of nano-wear on DLC coatings by AFM 62 (2013) 543–546.
[38] J. Furustig, I. Dobryden, A. Almqvist, N. Almqvist, R. Larsson, The Measurement of Wear Using AFM and Wear Interpretation Using a Contact Mechanics Coupled Wear Model, vol. 351, 2016, pp. 74–81.
[39] N.T. Garabedian, et al., Quantifying, locating, and following asperity-scale wear processes within multiasperity contacts, Tribol. Lett. 67 (2019) 1–10.
[40] C. Leriche, S. Franklin, B. Weber, Measuring multi-asperity wear with nanoscale precision, Wear 498–499 (2022), 204284.
[41] P. Spijker, G. Anciaux, J.F. Molinari, Relations between roughness, temperature and dry sliding friction at the atomic scale, Tribol. Int. 59 (2013) 222–229.
[42] F.-C. Hsia, et al., Rougher is more slippery: how adhesive friction decreases with increasing surface roughness due to the suppression of capillary adhesion, Phys. Rev. Res. 3 (2021), 43204.
[43] J. Liu, et al., Tribochemical wear of diamond-like carbon-coated atomic force microscope tips, ACS Appl. Mater. Interfaces 9 (2017) 35341–35348.
[44] A. Martini, S.H. Kim, Activation volume in shear - driven chemical reactions, Tribol. Lett. i (2021).

[45] Z.B. Milne, J.D. Schall, T.D.B. Jacobs, J.A. Harrison, R.W. Carpick, Covalent bonding and atomic-level plasticity increase adhesion in silicon-diamond nanocontacts, ACS Appl. Mater. Interfaces 11 (2019) 40734–40748.
[46] F. Hsia, F.M. Elam, D. Bonn, B. Weber, S.E. Franklin, Wear particle dynamics drive the difference between repeated and non- repeated reciprocated sliding Tribology International Wear particle dynamics drive the difference between repeated and non-repeated reciprocated sliding, Tribol. Int. 142 (2019), 105983.
[47] J. Du, S. Franklin, B. Weber, C. Author, A Force Controlled Tribometer for Pre-sliding Measurements at the Nanometer Scale, 2022, pp. 1–10.
[48] P.K. Hansma, et al., Tapping mode atomic force microscopy in liquids, Appl. Phys. Lett. 64 (1994) 1738–1740.
[49] D. Necas, P. Klapetek, Gwyddion : an Open-Source Software for SPM Data Analysis, vol. 10, 2012.
[50] M.H. Muser, et al., Meeting the contact-mechanics challenge, Tribol. Lett. 65–118 (2017).
[51] B. Weber, T. Suhina, A.M. Brouwer, D. Bonn, Frictional weakening of slip interfaces, Sci. Adv. 5 (2019) 1–8.
[52] K. Farain, D. Bonn, Non-monotonic dynamics in the onset of frictional slip, Tribol. Lett. 70 (2022) 1–5.
[53] U. Parlitz, et al., Identification of pre-sliding friction dynamics, Chaos 14 (2004) 420–430.
[54] M. Bazrafshan, M.B. Rooij, De Vries, E.G. De, D.J. Schipper, Evaluation of Pre-sliding Behavior at a Rough Interface : Modeling and Experiment, vol. 87, 2020.
[55] C. Xiao, et al., Threshold contact pressure for the material removal on monocrystalline silicon by SiO2 microsphere, Wear 376–377 (2017) 188–193.
[56] E.K. Antwi, K. Liu, H. Wang, A review on ductile mode cutting of brittle materials, Front. Mech. Eng. 13 (2018) 251–263.
[57] R. Komanduri, S. Varghese, N. Chandrasekaran, On the mechanism of material removal at the nanoscale by cutting, Wear 269 (2010) 224–228.
[58] P. Spijker, G. Anciaux, J.F. Molinari, Dry sliding contact between rough surfaces at the atomistic scale, Tribol. Lett. 44 (2011) 279–285.
[59] J. Jamari, Running-in of rolling contacts, Thesis 184 (2006).
[60] M. Scherge, The running-in of lubricated metal-metal contacts-a review on ultra-low wear systems, Lubricants 6 (2018).
[61] P.J. Blau, On the nature of running-in, Tribol. Int. 38 (2005) 1007–1012.
[62] R. Aghababaei, T. Brink, J.F. Molinari, Asperity-level origins of transition from mild to severe wear, Phys. Rev. Lett. 120 (2018) 1–6.
[63] S. Pham-Ba, T. Brink, J.F. Molinari, Adhesive wear and interaction of tangentially loaded micro-contacts, Int. J. Solid Struct. 188–189 (2020) 261–268.
[64] F.C. Hsia, et al., Contribution of capillary adhesion to friction at macroscopic solid-solid interfaces, Phys. Rev. Appl. 17 (2022) 1.
[65] J.F. Molinari, R. Aghababaei, T. Brink, L. Frérot, E. Milanese, Adhesive wear mechanisms uncovered by atomistic simulations, Friction 6 (2018) 245–259.
[66] H. He, et al., Subsurface structural change of silica upon nanoscale physical contact: chemical plasticity beyond topographic elasticity, Acta Mater. 208 (2021).
[67] W. Zhong, H. Wang, L. Ma, C. Zhang, Impact abrasive wear of Cr/W-dlc/DLC multilayer films at various temperatures, Metals 12 (2022).
[68] K. Zhao, R. Aghababaei, Interfacial plasticity controls material removal rate during adhesive sliding contact, Phys. Rev. Mater. 4 (2020) 1–7.
[69] Effect of Electrochemistry on Mechano-Tribo-Chemical Wear of Monocrystalline Silicon. Chen Xiao, Feng-Chun Hsia, Bart Weber, Steve Franklin, *Friction*accepted, 2023.